

EXPERIMENTAL AND NUMERICAL ANALYSIS OF THE TURBULENT FLOW IN T-SHAPE CHANNEL

Marian Branny, Michal Karch, Waldemar Wodziak
Marek Jaszczur, Remigiusz Nowak, Janusz Szmyd,
AGH University of Science and Technology, Kraków, Poland.
E-mail: marek.jaszczur@agh.edu.pl

Abstract

This paper presents a comparison between results obtained using experimental technique and computer simulation using two models: the standard $k-\varepsilon$ model and the RNG $k-\varepsilon$ model approach. An analysis has been performed to validate the turbulent models in T-shape channel which is commonly occurs in mining ventilation systems. The mean velocity and velocity fluctuation of the air flow inside the duct has been compared against the experimental results obtained using Particle Image Velocimetry and the reasonable agreement has been obtained.

Key words: T-shape channel flow, PIV

INTRODUCTION

In the mining the crossing of the longwall with the ventilation gallery creates a system of T-shape ventilation ducts. Flow and mixing at T-shape channel is also encountered in many industrial applications such as chemical reaction processes, combustion processes, piping systems of plant [1], [2], [3]. A model of the intersection of the mining face and ventilation gallery is shown in figure 1. While this geometry is apparently simple, the flows generated by it are often complex. Depending on the Reynolds number, a large separation zone can be formed, after the right corner of T-junction (see Fig.1). On the other hand on left side of T-junction (which actually has form of cavity) another recirculation zone of totally different behavior can be formed. The complexity of this recalculation zones makes the numerical prediction of the flow very difficult. The flow structure behind the right corner of T-junction itself is very complex from experimental point of view. Across the channel very large velocity at the top part of the channel and very low or negative velocity at the bottom part can be found therefore is not trivial problem for the good accuracy using PIV technique.

Numerous papers have been published on periodic, straight or L-shaped turbulent channel using a large variety of modeling techniques: RANS, URANS, LES, DLES and DNS [4 – 10]. However, there is no data available if L-shaped channel has additional arm which form T-shaped junction of closed channel (cave).

The application of interest in the present paper is investigations of air flow through the crossing of the mining longwall and ventilation gallery. The laboratory model is a certain simplification of a real object. Simplifications refer both to the object's geometry such as the rectangular shape of the cross-sections of workings, without mining face equipment as well as to the flow conditions such as the lack of air inflow from the goaf area. The investigated object consists of airways (headings) arranged in a T-shape. Maintained for technological reasons, the cave is exposed particularly to dangerous accumulations of methane. Properly arranged ventilation should assure the maintenance of methane concentrations at a safe level.

For this type of flows theoretical investigations is typically performed base on viscosity turbulence models with the standard k- ϵ model applied in the majority of cases [6],[7],[8].

The validation test of CFD simulation results for flow and methane concentration in the face area was done in the US [4][5]. Depending of the excavation system the authors indicated various models for the best way to simulate the real flow, namely, the RNG k- ϵ model, the k- ω model in the SST version and the Spalart-Allmaras model. The flow field, investigated in this paper differs significantly from those analyzed in the above mentioned papers where the connections between the ventilation ducts has been arranges differently.

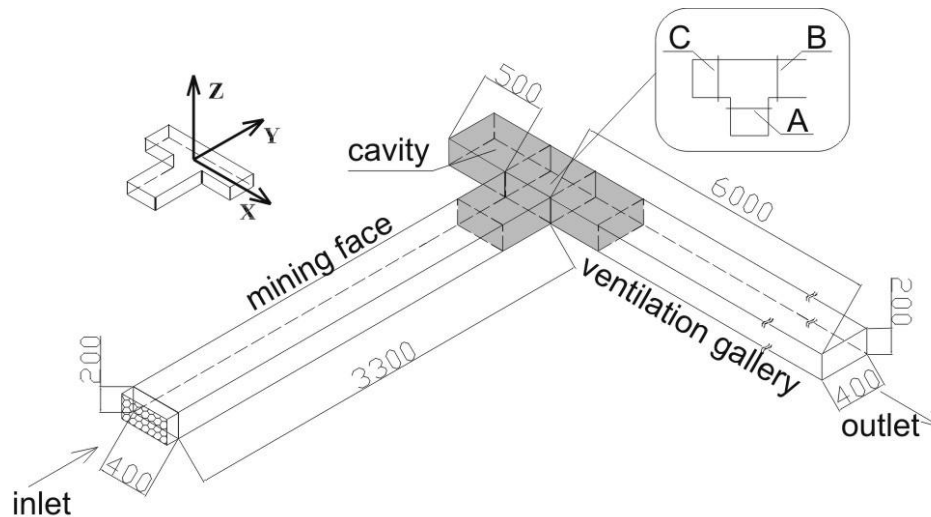


Figure 1. Experimental set-up of T-shape channel flow.

EXPERIMENTAL SETUP

The geometry with measurement section is shown in figure 1. Assuming that dimensions of the real object are: the cross-section of the duct 4m x 2m, the length of the cavity 5m, the length of inlet section (terminal segment of a mine face) 3.3 m and outlet 5.8m. The mean velocities are usually in the range of 1-2m/s (Reynolds number from 150000 to 300000). The geometrical scale of the physical model was 1:10. The air flow was assuming to be isothermal and statistically steady. In this case, equality of the Reynold's number in the model and the real object assures the flow criteria are similar. Having equal Re numbers ensures the averaged velocity fields are similar.

The inlet velocities were $U_1=3.8\text{m/s}$, and $U_3=9.85\text{m/s}$, the corresponding Reynolds numbers were equal to $Re_1=57300$, and $Re_2=148600$. Particle Image Velocimetry (PIV) method was used to evaluate the velocity vector components. The particles were illuminated with a double-pulse Nd:YAG laser and acquired by 4 Mpx monochromatic CCD camera. The double frame images were recorded a frequency of 3 Hz, and an overall time of one measure was of around 5 minutes.

The analysis of the influence of number of frames on the mean velocity component is presented in figure 2. Using that analysis for experiment measurement at least 1000 of uncorrelated flow fields has been used to obtain accurate statistic. Time Δt between two double frames varied from about $100\mu\text{s}$ to $500\mu\text{s}$, however, for the measurements inside the cave were the velocities are much lower that time was in the range of $3000\text{-}4000\mu\text{s}$, During the calculations, the size of interrogation windows that exhibit satisfying results was set to 32×32 px.

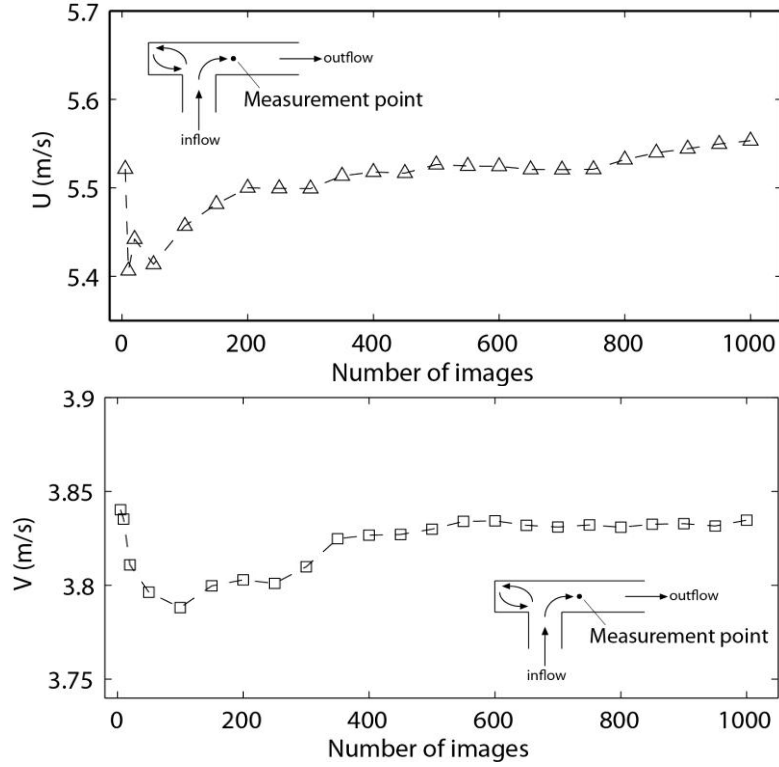


Figure 2. Wall-normal and streamwise velocity component versus number of samples to average procedure at $Re=148,600$.

MATHEMATICAL MODEL

Classical modeling of turbulence is based on the Reynolds concept, which for incompressible, and Newtonian fluids leads to the following equations:

$$\frac{\partial U_i}{\partial x_i} = 0$$

$$\frac{\partial U_i}{\partial t} + U_j \frac{\partial U_i}{\partial x_j} = -\frac{1}{\rho} \frac{\partial P}{\partial x_i} + \frac{\partial}{\partial x_j} \left(\nu \frac{\partial U_i}{\partial x_j} - \overline{u_i u_j} \right)$$

$$\frac{\partial C}{\partial t} + U_i \frac{\partial C}{\partial x_i} = \frac{\partial}{\partial x_i} \left(D \frac{\partial C}{\partial x_i} - \overline{u_i \phi} \right)$$

$$\overline{-u_i u_j} = \nu_t \left(\frac{\partial U_i}{\partial x_j} + \frac{\partial U_j}{\partial x_i} \right) - \frac{2}{3} \rho k \delta_{ij}$$

where $\nu_t = C_\mu \frac{k^2}{\varepsilon}$ - turbulent viscosity, k - kinetic energy, ε - dissipation rate of k , C_μ - constant, δ_{ij} - Kronecker delta

$$\frac{\partial k}{\partial t} + U_i \frac{\partial k}{\partial x_i} = \frac{\partial}{\partial x_i} \left(\left(\nu + \frac{\nu_t}{\sigma_k} \right) \frac{\partial k}{\partial x_i} \right) - u_i u_j \frac{\partial U_i}{\partial x_j} - \varepsilon$$

$$\frac{\partial \varepsilon}{\partial t} + U_i \frac{\partial \varepsilon}{\partial x_i} = \frac{\partial}{\partial x_i} \left(\left(\nu + \frac{\nu_t}{\sigma_\varepsilon} \right) \frac{\partial \varepsilon}{\partial x_i} \right) - C_1 \frac{\varepsilon}{k} u_i u_j \frac{\partial U_i}{\partial x_j} - C_2 \frac{\varepsilon^2}{k}$$

where $C_1, C_2, \sigma_k, \sigma_\varepsilon$ are constants

In this study, two models of turbulence were tested: the standard $k-\varepsilon$ model and a variation of that model, the RNG $k-\varepsilon$ model [10]. The RNG model differs from the standard version because it accounts for the additional source term in the transport equation for the rate of kinetic energy dissipation, thus describing the effects of the rapid rate of strain and streamline curvatures, and also because it uses a different method to compute the effective viscosity

The $k-\varepsilon$ RNG model is derived using a statistical technique called the renormalization group theory. Boundary conditions on rigid walls were set in the form of non-equilibrium wall functions. A numerical simulation of the air flow for conditions similar to experimental investigations was performed using FLUENT software. A structured, non-uniform mesh was generated for the computational domain. Local refinement was used in the cross-road region, where large gradients exist in the flow field and in the vicinity of the walls. Grid independence was examined with grid convergence index GCI. The order of magnitude of the GCI index is $10^{-2} - 10^{-3}$ for the two tested meshes of about 876,000 cells and another of 2,950,000 cells.

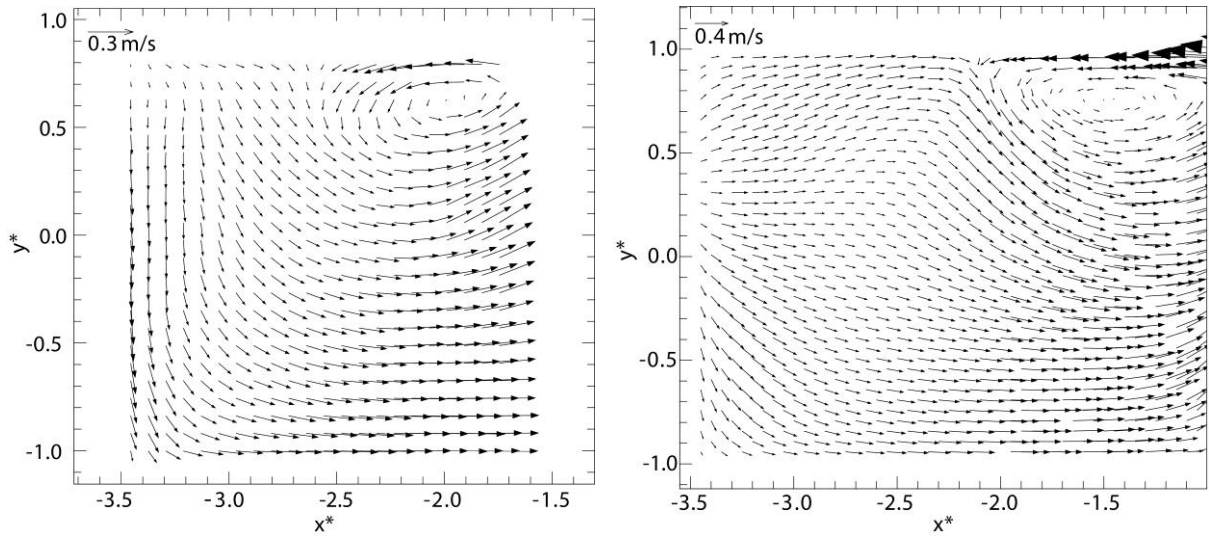


Figure 3. Flow fields obtained in the cave by experimental measurement(left) and numerical calculation (right) at $z^*=0$ and $Re=57300$

EXPERIMENTAL AND NUMERICAL RESULTS

The measurements and calculations were performed for two flow velocities: 3.8m/s and 9.85m/s (Reynolds numbers $Re=57300, 148600$). We present here only profiles of stream-wise and wall-normal components of velocities along the horizontal line at the half height of the channel ($z^*=0$) located before and after the cross of the ducts and in the cave. All geometrical dimensions are normalized by channel height. Figure. 3 shows a comparison of

the measured and calculated velocity in the cave at $z^*=0$ and $Re=57300$. Figure 4 shows visualization of velocity vectors map of T-shape channel flow at $z^*=0$ and $Re=57300$ obtained using Particle Image Velocimetry by connection of results from individual measurement PIV sections.

Figure 5 and 6 show the velocity for the cross section A, C and B and for Reynolds number $Re=57300$ (Fig.5) and $Re=148600$ (Fig.6). Small differences between the measurements and calculation results for the stream-wise and wall normal components for two considered flow velocities can be seen for the entrance section A and large difference for wall normal velocity components for section B, and C. Also numerical predictions itself differs a lot depending on model in that area. The calculated values of streamwise velocity components over-predict the measured ones by about two times whereas the wall normal components differ even in the shape of its profile. Note that the flow field in this zone is complex and even a slight translation of the horizontal line in the x direction changes the profile of the transverse component considerably. For section B the predicted velocities are in good agreement with the experimental results in the main stream but differ in the separating zone. The calculations over-predict the negative streamwise components of velocity in the zone where recirculation occurs.

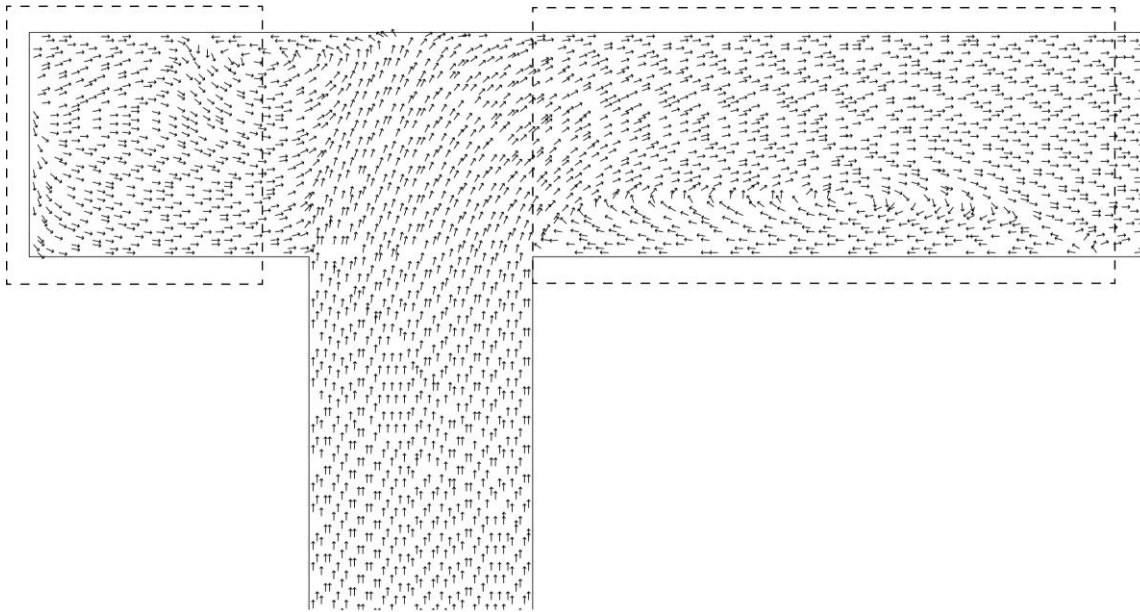


Figure 4. Vectors map of global velocity distribution in the experimental channel for $Re = 57300$, and at $z^*=0$ obtained from connection of results from individual measurement sections (in presented figure the cavity section and recirculation section are marked).

The comparison of numerical results (the standard $k-\varepsilon$ model and a variation of that model, the RNG $k-\varepsilon$) with measurements (PIV experiment) is shown in figure 7 and 8 for Reynolds number $Re=57300$. Figure 7 presents the distribution of normal stresses ($\overline{u_x^2}, \overline{u_y^2}, \overline{u_z^2}$) for the cross section C, this is shown in non-dimensional form $\overline{u_x u_x} / \overline{U}^2, \overline{u_y u_y} / \overline{U}^2, \overline{u_z u_z} / \overline{U}^2$. Figure 8 presents the distribution of shear stresses ($\overline{u_x u_y}, \overline{u_x u_z}, \overline{u_y u_z}$) for the cross section C, this is shown in non-dimensional form $\overline{u_x u_y} / \overline{U}^2, \overline{u_x u_z} / \overline{U}^2, \overline{u_y u_z} / \overline{U}^2$.

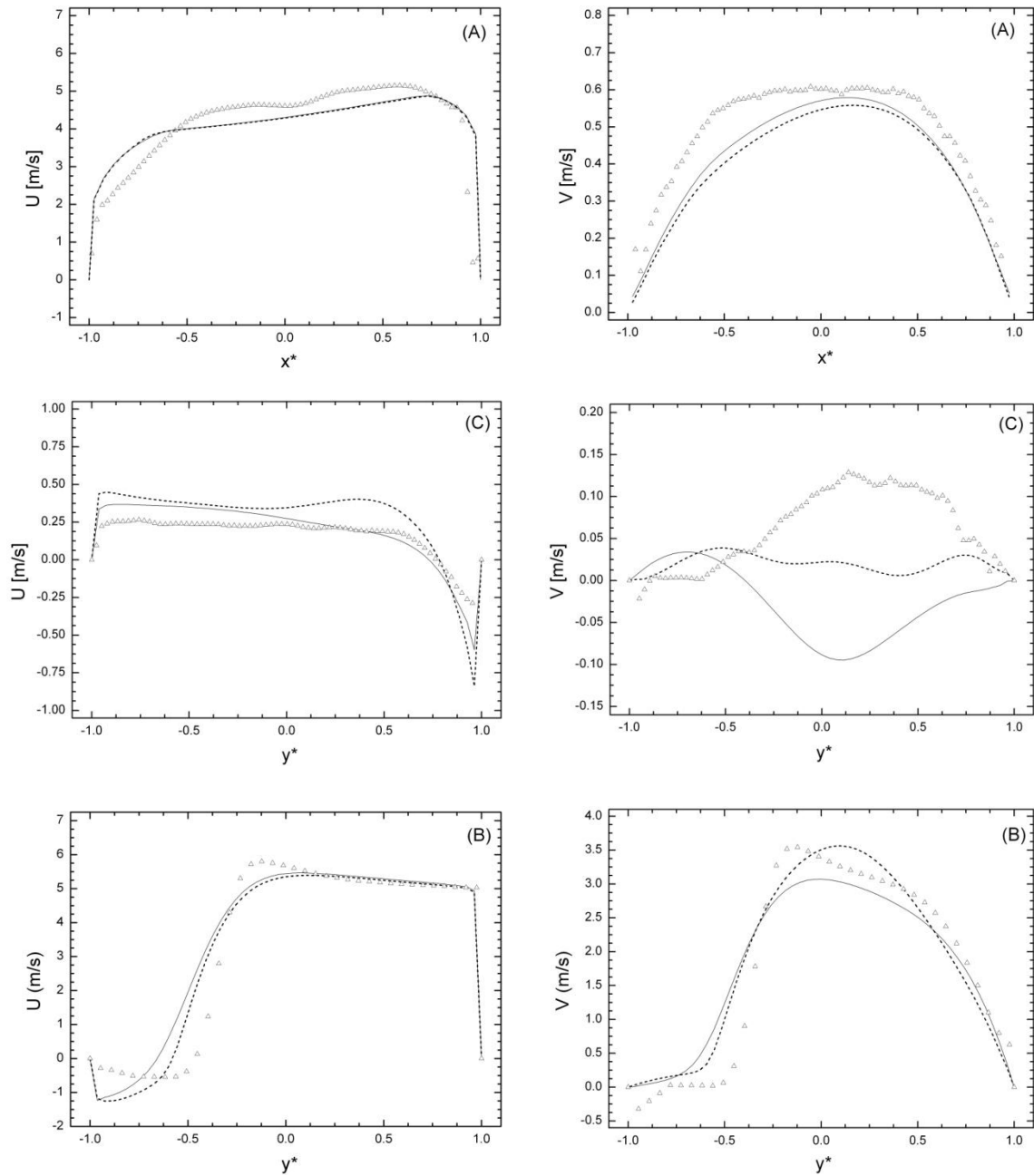


Figure 5. Flow streamwise (left) and wall-normal (right) velocity component for section A, C and B at $z^*=0$ and $Re=57300$ (—) $k-\epsilon$, (---)RNG $k-\epsilon$, (Δ)Exp.

From these figures, the flow characteristics agree qualitatively with one another. The high value of normal stresses exhibits near the middle part of the recirculation zone and keeps large values downstream (Fig. 7). On the other hand, high values of shear stresses is observed not only in the shear layer but also along mixing interfaces (Fig.8).

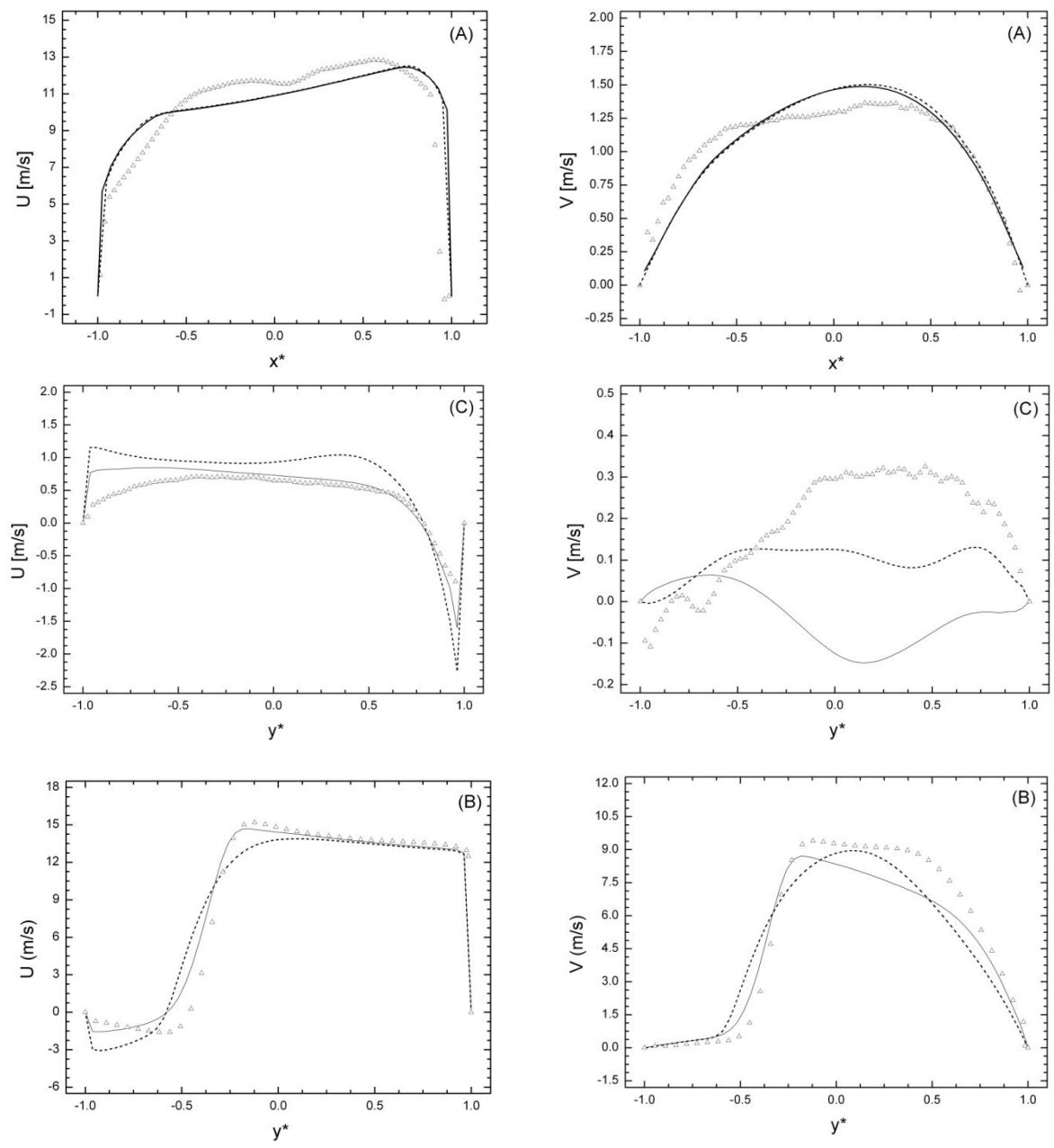


Figure 6. Flow streamwise (left) and wall-normal (right) velocity component for section A, C and B at $z^*=0$ and $Re=148600$ (—) $k-\epsilon$, (- - -)RNG $k-\epsilon$, (Δ)Exp.

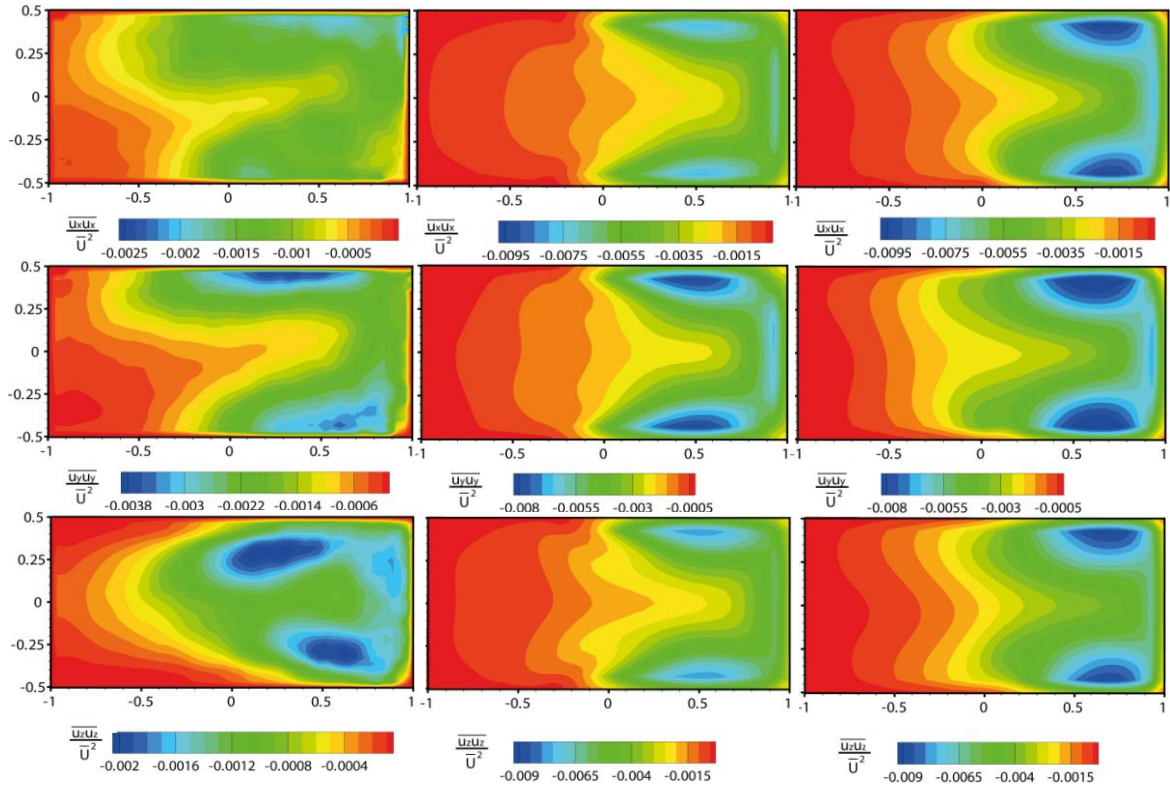


Figure 7. The distribution of normal stresses for Re=57300 and section C, (left part) experiment, (central part) numerical results $k-\epsilon$ model (right part) RNG $k-\epsilon$ model

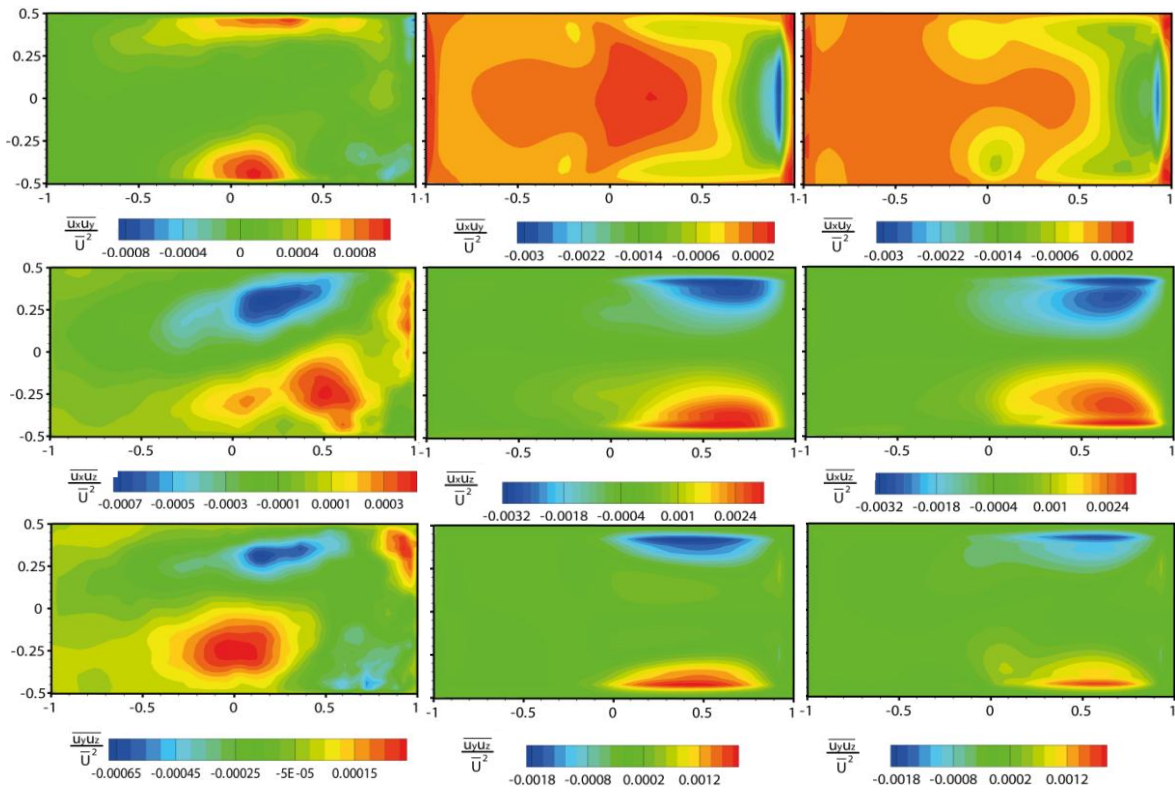


Figure 8. The distribution of shear stresses for Re=57300 and section C, (left part) experiment, (central part) numerical results $k-\epsilon$ model (right part) RNG $k-\epsilon$ model

CONCLUSIONS

The transport phenomena of the turbulent air flows inside a T-shape channel junction system have been studied using PIV and numerical simulation. Experimental data has been used to validate the numerical results based on turbulence models. In this paper, a two-equation $k-\varepsilon$ and RNG $k-\varepsilon$ turbulence model were tested with air flowing through the laboratory model representing a fragment of a mining ventilation network. Some difference between results and models has been obtained. The examined flow is characterized by such flow features as separation, stream impingement on the wall, stress-driven flow and strong streamline curvature. Neither tested model, the standard $k-\varepsilon$ and RNG $k-\varepsilon$, provided satisfactory results for the examined flow in the cave zone. Furthermore, the calculated values of streamwise components are over-predicted in the cave zone. This will cause the ventilation intensity to be overestimated in this area. For the cross section located before and behind the cross of the ducts, the calculations and measurements are in quite good agreement with the experimental results, bearing in mind the accuracy needed in ventilation problems. However, considerable differences are observed in the separation zone

ACKNOWLEDGEMENTS

The research was supported by the Polish Ministry of Science and Higher Education project No. 4653/B/T02/2010/39)

REFERENCES

1. Nakayama, H., Hirota, M., Shinoda, K., Koide, S.,(2005): *Flow Characteristics in a Counter-Flow Type T-junction*, Thermal Science and Engineering, Vol.13, pp. 17-23
2. Kelso, R. M., Lim, T. T., Perry, A. E., (1996): *An experimental study of round jets in cross-flow*, Journal of Fluid Mechanics, Vol.306, pp.111–144
3. Haven, B. A., Kurosaka, M., (1997): *Kidney and anti-kidney vortices in crossflow jets*, Journal of Fluid Mechanics, Vol.352, pp.27-64
4. Wala, A. M., Vytla, S., Taylor, C.D., Huang, G., (2007): *Mine face ventilation: a comparison of CFD results against benchmark experiments for CFD code validation*, Mining Engineering, Vol.59, pp.10-17
5. Wala, A.W., Stoltz, J.R., Jacob, J.D., (2001): *Numerical and experimental study of a mine face ventilation system for CFD code validation*, Proceedings of the 7th International Mine Ventilation Congress, Krakow. pp.411-418
6. Krawczyk, J., (2007): *Jedno i wielowymiarowe modele niestacjonarnych przepływów powietrza i gazów w wyrobiskach kopalnianych. Przykłady zastosowań*. Kraków, Wydawnictwo Instytutu Mechaniki Górotworu PAN.
7. Aminossadati, S.M., Hooman, K., (2008): *Numerical simulation of ventilation air flow in underground mine workings*, 12th U.S./North American Mine Ventilation Symposium, pp.253-259
8. Silvester, S.A., (2002): *The integration of CFD and VR methods to assist auxiliary ventilation practice*. PhD thesis, The University of Nottingham.
9. Jaszczur, M., Portela, L., (2008): *Numerical data for reliability of LES for non-isothermal multiphase turbulent channel flow*, Quality and reliability of LES pp. 343-354
10. Kuan, B., Yang, W., Schwarz, M.P.,(2007): *Dilute gas-solid two-phase flows in a curved 90° duct bend: CFD simulation with experimental validation*, Chemical Engineering Science, Vol.62, pp.2068-2088